A Performance Assessment of a Developed Mesh-Generating Algorithm: A Computer-Aided Design Modelling Process to Support Progression within Additive Manufacturing

J.A. GARDNER[1], G.A. BINGHAM[1], A.M. PATERSON[1]
[1]Loughborough Design School, Loughborough University, Loughborough, UK
j.a.gardner@lboro.ac.uk, g.a.bingham@lboro.ac.uk, a.m.paterson@lboro.ac.uk

ABSTRACT
Developments in Additive Manufacturing (AM) technologies and associated processes have increased the limits of attainable design complexity, yet Computer-Aided Design (CAD) tools that may utilise these new potentials have not advanced as rapidly. Research detailed in this paper addresses aspects of automatic geometric design that may support the generation of high resolution, functional, three-dimensional (3D) textures. A 3D CAD model of a surface with complex curvature was modelled to be systematically populated with points using a developed mesh-generation algorithm. Following the successful generation of a mesh the distances between points were analysed, throughout the process, to measure the performance of the algorithm. Equidistance between points was achieved and, if the algorithm was used as intended, would provide an essential foundation for successive texture application processes with minimal manual input required.

KEYWORDS: Mesh generation; Computer-Aided Design; Additive Manufacturing; functional textures; biomimetics

1. INTRODUCTION

Traditional texture application processes are manual, completed after parts are formed, and involve hand-carving geometries, such as paint scratching and roller printing, directly into parts [1]. These processes have since been replaced by CAD software equivalents that generate data to be interpreted by Computer-Aided Manufacturing (CAM) machinery [2]. CAM machinery presses or mills material of parts after they are formed or mould surfaces beforehand [3]. Generating textures using these processes restricts the complexity of the geometries that may be produced due to the difference in malleability and viscosity between materials when they molten and solid [4]. Molten materials are able to flow into small volumes of mould cavities, however, the solidification process makes it impossible to remove 3D textures whilst keeping them intact with surfaces, due to mechanical restrictions [5].
AM technologies and related processes allow for more complex textures (Figure 1) to be fabricated, therefore allowing designers and engineers to produce parts with a wider range of functionalities [6]. Texture functionality types are various and because of this their geometries are determined by the conditions of their intended applications [7]. Hydrophobic surfaces utilise liquid surface tension to repel water and contaminants; hydrodynamic surfaces control fluid flow within boundary layers to reduce total drag; non-excreting adhesive surfaces deform their geometries around features of other surfaces to utilise Van der Waals forces [8].

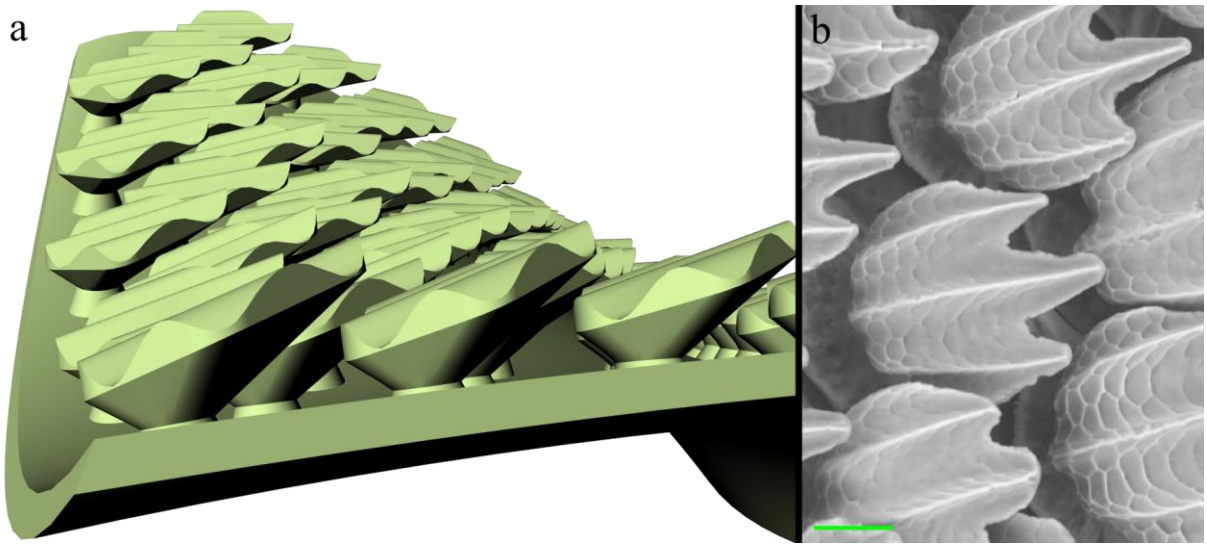

Figure 1: Examples of geometric complexity of 3D textures on (a) a CAD model and (b) a bonnethead shark – scale: 50µm [9]

Examples of these functional surfaces may be found in nature and have been experimented on to highlight the significant advantages functional textures provide surfaces [7]. A frequently researched functional texture is shark skin due to its relatively large structure size as well as the potential range of applications that may benefit from having them [6,9]. Shark skin structures, or denticles, are solid geometries that reduce total drag force, by approximately 10%, to maintain high swimming velocities [6]. As well as individual structure form, structure positioning is a key determinant of functional texture performance [10]. Gaps between structures cause fluid behaviours to change and generate turbulence outside boundary layers which reduces functional texture performance [11].

Previous shark skin emulation attempts have incrementally increased the percentage improvement the textures make against comparable functional surfaces [6]. The first notable attempt consisted of a simple pattern of embossed ellipses on a planar surface [12]. A subsequent attempt involved a shark skin inspired high performance swimsuit that controlled fluid flow using the weave pattern of the fibres [13]. The attempt that most closely matches shark skin involves the fabrication of similar structure geometries using Multi-Jet Modelling [6]. Although this research demonstrated that complex textures can now be generated, with the inclusion of AM, the structures were tenfold larger than shark skin structures and were positioned in a rectangular array and therefore did not overlap. A flexible substrate was also used to provide curvature to the textured surface; therefore high fidelity shark skin is yet to be generated directly onto a 3D CAD model or a physical model.

AM now allows nature's functional surfaces to be emulated, however, there are no CAD modelling methods that support the generation of high fidelity texture data on surfaces with unrestricted curvature [14]. There are, however, some CAD modelling methods that involve processes that may be used to generate 3D texture CAD data [15,16]. To address this gap a novel CAD modelling method was developed so that the progression made in manufacturing technologies is matched by software that enables them. Research detailed within this paper entails the generation of point and vector data to position structures to form shark skin, or other, functional textures on surfaces with non-planar, complex curvatures.

2. EXPERIMENTAL PROCEDURE

A surface CAD model (Figure 2a) was created using Rhinoceros 3D and Grasshopper CAD software to test the performance of the point generation section of a system designed to generate 3D functional texture data [17,18]. Four boundary curves, of identical length and curvature, were drawn to form a quadrilateral surface with complex, non-planar curvature. A curvature analysis (Figure 2c) was performed to assess which areas of the CAD model exhibited tight curvature. Values shown in the key (Figure 2b), which detail the range of curvature across the surface, were recorded to assist in attributing mesh point generation performance with respect to surface curvature.

Mesh points are to be used as attachment locations for structures, therefore the distances between them should relate to the sizes of structures that neighbour each point. As surface structure size is relatively uniform across textures the distances between attachment locations should also be.

A meshing algorithm of the authors' creation was employed to populate points across the surface CAD model. Initially a target equidistance value was set – one distance unit – relative to the distance between boundary curve end points – 100 distance units. The units of distance used were not recorded as the surface CAD model may be scaled, uniformly, by the same factor as the mesh points positions if the same scaling origin coordinates are used. The target equidistance value was used to generate all points within the mesh, by referencing points generated within preceding iterations, until the surface CAD model was populated by points and the algorithm termination condition was satisfied.

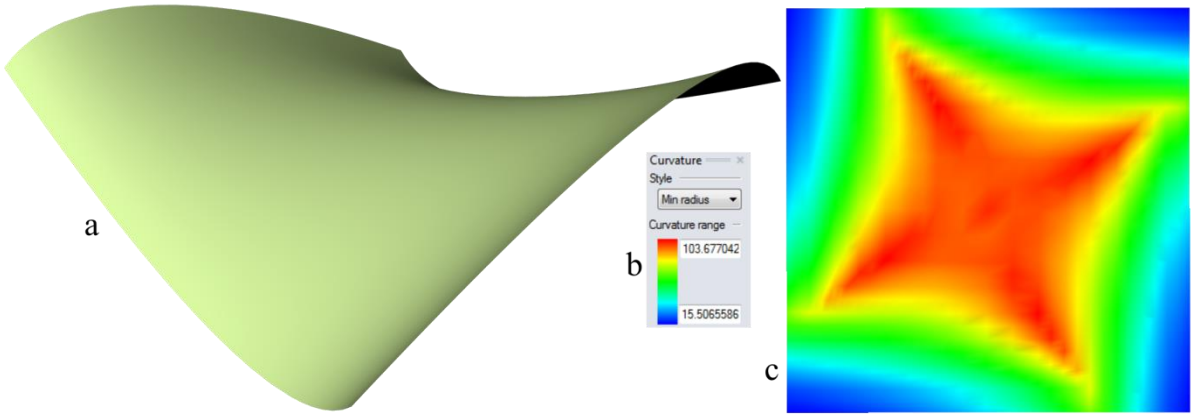

Figure 2: (a) Surface CAD model used to test meshing algorithm with a (b) curvature analysis of the surface and an accompanying (c) colour-curvature key

Each mesh point was processed automatically, within all iterations of the mesh generation process, to identify which points were closest to each other record the linear distance between them. Therefore the total number of distances recorded equals the number of mesh points in all iterations. Minimum and maximum distances were recorded for all iterations, and means average distances were also calculated.

3. RESULTS

All distance data is displayed in a table (Table 1) and a line graph (Figure 3), which is accompanied by dashed lines that may be used to assist in determining at what stages in the mesh generation process the algorithm's performance changes.

Iteration No.	No. of points	Min. dist. (%)	Max. dist. (%)	Mean avg. dist. (%)	Filtered min. dist. (%)	Filtered max. dist. (%)
1	19	99.98	99.99	99.98	99.98	99.99
20	1387	99.77	100.11	99.97	99.79	100.10
40	5167	98.39	101.50	99.89	98.47	101.13
49	7649	96.12	102.56	99.78	96.44	102.15
54	9099	94.24	103.05	99.68	94.65	102.70
60	10211	93.83	103.74	99.72	94.35	103.09
70	11091	60.02	105.07	99.72	94.10	103.29
78	11250	60.48	103.70	99.61	89.60	103.15

Table 1: Closest mesh point distance data

Mean average values are consistent throughout the mesh point generation process and culminate at 99.61% of the target equidistance value. Minimum and maximum distance values deviate throughout the mesh generation process, but significantly near boundary curves and whilst points are generated on extreme surface curvature; these key stages are reported and highlighted in Table 1 and Figure 3 respectively.

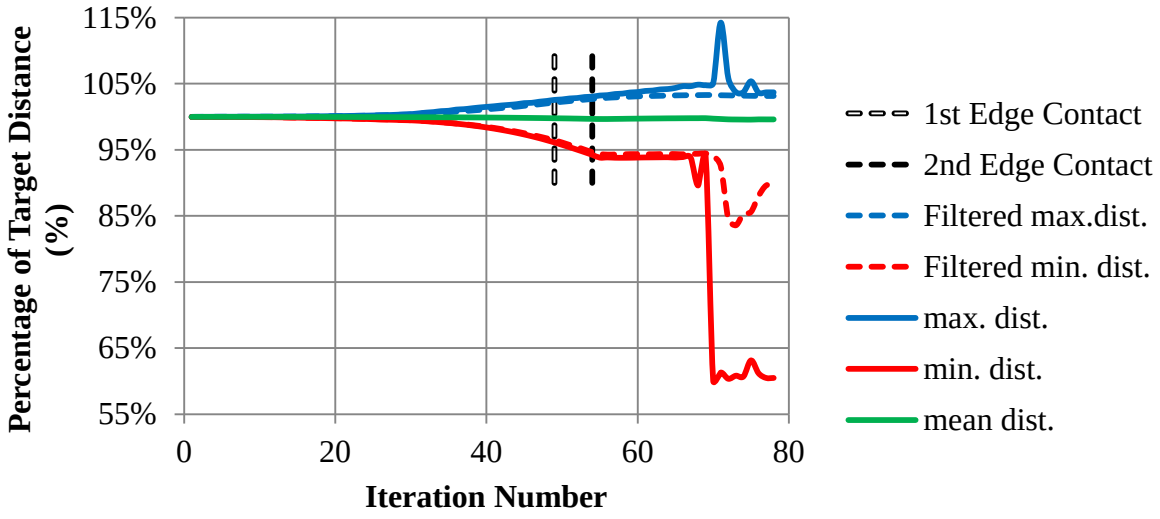

Figure 3: Graph of closest point measurements of meshed surface CAD model

Dashed lines highlight the stages of the mesh generation process where boundary curves begin to determine mesh performance. These stages are also displayed to help determine where divergence from equidistance occurs (Figure 4).

High numbers of points per iteration and the requirement of high numbers of iterations to be calculated, to generate a complete mesh, cause the process to be computationally demanding. To understand this demand the numbers of points within all iterations is displayed in a graph (Figure 5). References are used to highlight how the numbers of points per iteration change according to the boundaries that define the surface CAD model. The number of points exponentially increases until the first boundary curve interacts with the points, which is followed by iterations of constantly increasing point numbers. This pattern changes when all boundary curves interact with mesh points to cause the numbers of points to plateau; finalising at 11250 mesh points. The total run time of the mesh-generating algorithm was 18

minutes 51 seconds and generated a total of 431565 points; therefore approximately 380 points were generated each second.

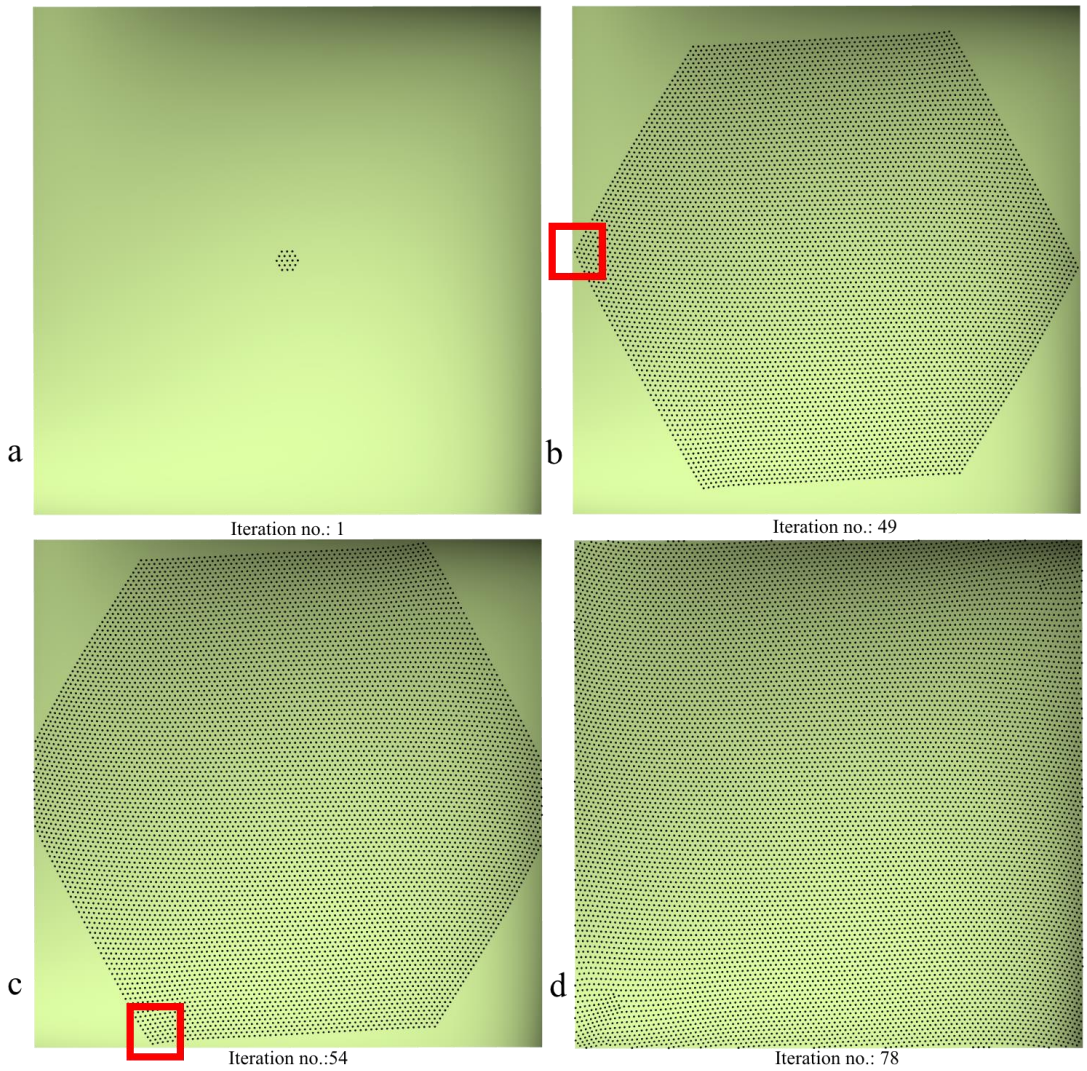

Figure 4: Key stages of the meshing process, including (a) initial mesh point generation, (b) first interaction between a point and a surface edge, (c) interaction between a point and a perpendicular surface edge, and (d) meshing completion

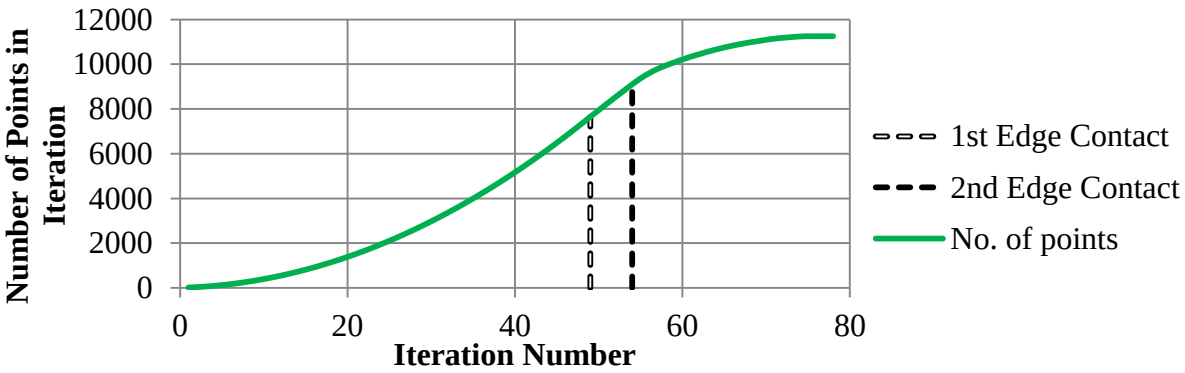

Figure 5: - Graph of the number of points generated in each iteration

4. DISCUSSION

Performance of the mesh-generating algorithm was principally assessed using the linear distances between neighbouring points as a key performance indicator. A complete mesh was generated as all areas of the surface CAD model were populated by points (Figure 6a).
Throughout the mesh generation process the mean average distances were stable (Figure 3), despite deviations from the target equidistance value. This result is mainly caused by the data being highly concentrated about the mean average, but also due to larger distances on one side of a point creating smaller distances on the other.
Closest point minimum distances and maximum distances, begin to decrease and increase, respectively, at approximately iteration 30, which coincides with mesh points propagating on areas with relatively higher surface curvature acceleration. In one direction points were splayed whereas in the perpendicular direction they were restricted.
Minimum and maximum distances between closest points continued to deviate from the target equidistance and were unaffected by the initial boundary curve interaction between a boundary curve and a point (Figure 4b). This divergence pattern was altered by the interaction of a subsequent boundary curve (Figure 4c) which caused the stabilisation of distances between points. Differences between mesh generation performances occurred due to the number of points being processed in areas with tighter surface curvature. This effect may also be caused by the relative angles generated between the outer most points and the boundary curves that interact with them; lower relative angles have a higher probability of causing equidistance diversion. At the stage when these mesh points are influenced by the edges the reduction in meshing performance ceases and stabilises.
A further significant reduction in performance occurs when mesh points are generated in new positions, in iteration 70, due to the points being in the area of tightest curvature across the CAD model. Differences between linear distances and the shortest distances along a surface, between points, are larger on areas of tight curvature. These differences cause coordinate averaging issues and result in points being introduced between points (Figure 6b). The new minimum closest distance remains at approximately 60% as the pair of closest points propagate towards the centre of the surface CAD model. As this pair of closest points propagates further towards the centre of the surface the distances between points, nearest the most extreme surface curvature, begin to return to the target equidistance value due to coordinate value averaging.

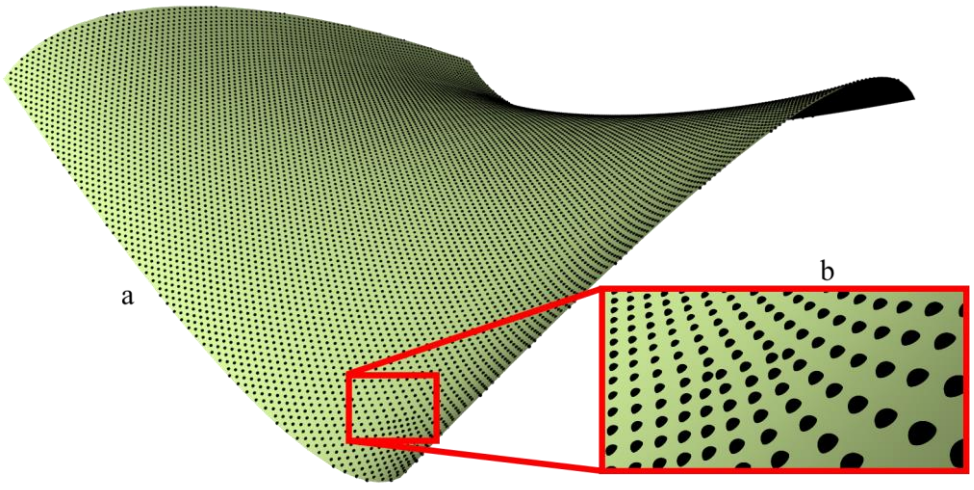

Figure 6 - (a) A meshed surface CAD model with (b) a magnified view of points generated on relatively tight surface curvature

In iteration 70, a significant decrease in minimum closest distance occurs. This occurrence increases the maximum closest distance between points, in the subsequent iteration, as points begin to return to their previous positions.
The use of a filter, which removes a number of distances at either end of the ordered values, generated new datasets that approximately follow a similar pattern to the unfiltered datasets until iteration 70. At the stage where points are generated on the tightest surface curvature, the effect of additional mesh points only affects relatively few distances. The effect may be seen by the significant difference between filtered and unfiltered minimum distances in the final iterations of the process, finishing at 89.60%. As there are relatively low numbers of points that are far from the target equidistance value, therefore it is feasible for manual point position manipulation to be considered before they are used as structure attachment locations. Filtered maximum distances between closest points were also more stable after iteration 70, suggesting that there were few relatively large gaps generated by additional mesh points at this stage.
The difference in number of points between iterations is directly proportional to the ratio of unmeshed surface area and the points, within the target equidistance value, which may be used as references to generate new points. If all existing points may be used to generate new points the rate of change between unmeshed and meshed surface area is constant. In iterations including boundary curves that influence mesh point generation this rate of change alters causing a plateau until mesh completion (Figure 5). As 380 point positions may be calculated each second whilst maintaining a consistent mean average that approximately matches the target equidistance value (99.61%), using this process requires significantly less time than manual positioning of structure attachment locations.

5. CONCLUSIONS

To assess the performance of a mesh-generating algorithm, a sample surface CAD model was systematically populated with points so that the distances between them could be measured. Analysis of the distances proved the process to successfully generate mesh points, which require relatively low manual modification, and may be used as attachment locations for structures to form 3D functional textures. The developed mesh-generating algorithm may be used to utilise the potential of AM technologies, which other manufacturing techniques cannot offer, as well as reducing the time required to generate 3D texture data.

REFERENCES

[1] Williams, R., & Sheldon, C. (2009). Texture your surface. *Robin williams handmade design workshop: Create handmade elements for digital design* (pp. 31-231). Berkeley, California: Peachpit Press.

[2] Mould-tech. (2016). Retrieved from http://www.mold-tech.com/

[3] Bixler, G. D., & Bhushan, B. (2013). Bioinspired micro/nanostructured surfaces for oil drag reduction in closed channel flow. *Soft Matter, 9*, 1620-1635. doi:10.1039/c2sm27070f

[4] Sha, B., Dimov, S., Griffiths, C., & Packianather, M. S. (2007). Investigation of micro-injection moulding: Factors affecting the replication quality. *Journal of Materials Processing Technology, 183*(2-3), 284-296. doi:10.1016/j.jmatprotec.2006.10.019

[5] Yao, D., & Kim, B. (2004). Scaling issues in miniaturization of injection molded parts. *Journal of Manufacturing Science and Engineering, 126*(4), 733-739. doi:10.1115/1.1813479

[6] Wen, L., Weaver, J. C., & Lauder, G. V. (2014). Biomimetic shark skin: Design, fabrication and hydrodynamic function. *The Journal of Experimental Biology, 217*(10), 1656-1666. doi:10.1242/jeb.097097

[7] Malshe, A., Rajurkar, K., Samant, A., Hansen, H. N., Bapat, S., & Jiang, W. (2013). Bio-inspired functional surfaces for advanced applications. *CIRP Annals - Manufacturing Technology, 62*(2), 607-628. doi:10.1016/j.cirp.2013.05.008

[8] Aradya, S. V., Frei, M., Hybertsen, M. S., & Venkatereman, L. (2012). Van der waals interactions at metal/organic interfaces at the single-molecule level. *Nature Materials, 11*, 872-876. doi:10.1038/NMAT3403

[9] Oeffner, J., & Lauder, G. V. (2012). The hydrodynamic function of shark skin and two biomimetic applications. *The Journal of Experimental Biology, 215*, 785-795. doi:10.1242/jeb.063040

[10] Dean, B., & Bhushan, B. (2010). Shark-skin surfaces for fluid-drag reduction in turbulent flow: A review. *Philosophical Transactions of the Royal Society, 368*(1929), 4755-4806. doi:10.1098/rsta.2010.0201

[11] Wen, L., Weaver, J. C., Thornycroft, P. J. M., & Lauder, G. V. (2015). Hydrodynamic function of biomimetic shark skin: Effect of denticle pattern and spacing. *Bioinspiration & Biomimetics, 10*(6), 1-13. doi:10.1088/1748-3190/10/6/066010

[12] Inspired by Nature The discovery of sharklet. (2016). Retrieved from http://sharklet.com/our-technology/sharklet-discovery/

[13] Polley, M. (2015). Knitting and the olympic games: Clothing, competition, culture, and commerce. *Textile, 12*(1), 72-85. doi:10.2752/175183514x13916051793514

[14] Tanaka, F. (2011). Current situation and problems for representation of tolerance and surface texture in 3D CAD model. *International Journal of Automation Technology, 5*(2), 201-205.

[15] Bingham, G. A. (2007). *The generation of 3D data for rapid manufactured textiles.* (Unpublished Ph.D.). Loughborough University, Loughborough University. (ALEPH 001178147)

[16] Bingham, G. A., & Hague, R. (2013). Efficient three dimensional modelling of additive manufactured textiles. *Rapid Prototyping Journal, 19*(4), 269-281. doi:10.1108/13552541311323272

[17] Robert McNeel & Associates. (2015). *Rhinoceros 3D* (Version 5)

[18] Robert McNeel & Associates. (2009). In Rutten D. (Ed.), *Grasshopper* (Version January-27, 2014)